Available online at www.sciencedirect.com
ScienceDirect
Journal of Sound and Vibration 307 (2007) 187–201
JOURNAL OF SOUND AND VIBRATION
www.elsevier.com/locate/jsvi

Vibration control of an inverted pendulum type structure by passive mass–spring-pendulum dynamic vibration absorber

N.D. Anh[a,*], H. Matsuhisa[b], L.D. Viet[a], M. Yasuda[c]

[a]*Institute of Mechanics, Vien Co hoc, 264 Doi Can, Hanoi, Vietnam*
[b]*Department of Precision Engineering, Kyoto University, Kyoto 606-8501, Japan*
[c]*Tokkyokiki Corporation, Amagasaki City, Hyogo 660-0833, Japan*

Received 1 November 2006; received in revised form 27 June 2007; accepted 30 June 2007

Abstract

In this paper, the vibration reduction for a stable inverted pendulum with passive mass–spring-pendulum-type dynamic vibration absorber (DVA) is investigated. Results obtained contain the conventional pendulum systems as a special case. Equivalent mass ratio established shows that the DVA on an inverted pendulum is more effective than the DVA on a normal pendulum system. Parameters of the DVA are determined by maximizing the damping characteristic of the combined system. The location, where the DVA has no effect is specified. Numerical simulation is done in an example of the inverted pendulum structure in the ocean. A mass–spring inverted-pendulum-type DVA is proposed to reduce the required length of the conventional mass–spring-pendulum-type DVA. The cell-to-cell mapping method is used in the numerical simulation to determine the nonlinear stability domain.

1. Introduction

The problem of undesired-vibration reduction is known for many years and it has become more attractive nowadays.

A tuned-mass damper (TMD), or dynamic vibration absorber (DVA), is found to be an efficient, reliable, and low-cost suppression device for vibrations caused by harmonic or narrow-band excitations. This device comprising a mass, springs, and viscous damper was proposed in 1909 and has been widely used in many fields of engineering.

Since mass ratio of TMD to the primary structure is usually few percent, in TMD design stiffness and damping ratio can be determined by balancing the two fixed points in the frequency response, in the case of harmonic excitation, or by minimizing the mean-square response under random excitation, or by balancing the poles of system [1–6]. It should be noted that in the classical theory of TMD the primary structure is modeled as a spring–mass system. However, other models also are of much interest in research and engineering applications. In particular, pendulum-type systems occurring as a model of solid body with a fixed

*Corresponding author.
E-mail address: ndanh10000@yahoo.com (N.D. Anh).

0022-460X/$ - see front matter © 2007 Elsevier Ltd. All rights reserved.
doi:10.1016/j.jsv.2007.06.060

fulcrum point can play an important role in many fields such as machinery, transportation, and civil engineering.

The planar pendulum has been used to illustrate many of the basic features of dynamics. When it is periodically forced, the pendulum can undergo an array of changes in state, including chaotic behavior. Its importance has equally been demonstrated by many problems of practical interest that result in mathematical models which incorporate aspects of a pendulum-like equation in one form or another; for instance, the heave-excited roll response of a ship in waves.

The dynamic absorber for wind-induced vibration of ropeway carriers was investigated theoretically by Matsuhisa [7]. The ropeway carrier can be regarded as a rigid-body pendulum and the theory of location was established in 1993. The theory indicates that the effectiveness is proportional to the square of the distance of the absorber from the center of oscillation. Consequently, the effectiveness of the dynamic absorber depends much on its location. In the case of gondola, the center of oscillation is around the midpoint between the center of gravity and the bottom of the gondola. It means that the absorber at the bottom of gondola does not work well. The absorber must be located as high as possible, and even if the absorber is at the fulcrum, it works very well. The world's first in the world installation of the dynamic absorber on the ropeway chair lifts was in 1995 and at present they have been installed about 20 ropeways in Japan.

As mentioned above, the pendulum-type systems are of much interest in research and engineering applications. Hence, the problem addressed in this paper is how to extend the theory of location [7] as much as possible to those systems. In fact, an alternative class of pendulum systems is the so-called inverted pendulum and it is well-known. The research phenomena involved in inverted-pendulum systems are much challenging compared to conventional pendulum-type ones, as the first can be stable or unstable while the latter can only be stable. The (single and multiple) unstable inverted pendulum is an example dealing with classical, as well as modern, control and with Robotics. It is challenging to design/tune stabilizing controllers for this inherently unstable system [8–13]. The base-excited inverted pendulum has occurred in many control problems [14–17]. An aspect in the study of human locomotion is to simulate the unstable equilibrium of the trunk about the upright position and to relate to the control law that human use during walking. The human trunk is modeled as an inverted pendulum with up to 3° of rotational freedom. The base point of the pendulum corresponds to the center of the pelvis and is allowed to move in three directions [17]. The problem ''man–machine'' closely related to the balancing of an inverted pendulum has noteworthy consequences in biology, which relates to the explanation of self-balancing of the human body [18,19] or in the construction of biped robots [20,21].

The stable inverted-pendulum-type systems can be an adequate model in civil engineering. The model of beam supported by a linear-elastic torsion spring at one end and with a point mass at the other end is representative of numerous applications, for example, in the analysis of the dynamic response of soil–structure [22] or fluid–structure interactions [23]. The soil–structure interaction can be modeled by tension springs while in the fluid–structure interaction the torsion springs are due to buoyancy forces. If the bending stiffness of the beam is large enough, one may use the model of inverted pendulum with a linear-elastic torsion spring. In Ref. [23], the response of an articulated tower in the ocean subjected to deterministic and random wave loading was investigated. The tower was modeled as an upright rigid pendulum with a concentrated mass at the top and having one angular degree of freedom about a hinge with Coulomb damping which can be replaced approximately by an equivalent linear viscous one. Compliant platforms such as articulated towers are economically attractive for deep-water conditions because of their reduced structural weight compared to conventional platforms. The foundation of the tower does not resist lateral forces due to wind, waves, and currents; instead, restoring moments are provided by a large buoyancy force, a set of guy-lines or a combination of both [24–27].

It should be noted that in all above-mentioned researches, the use of dynamic absorbers as an additional tool for vibration control was not considered. Thus, the control problem of unstable and stable inverted-pendulum-type systems using different kinds of dynamic absorbers such as passive, semi-active, and active ones might be an aspect of high interest.

In the paper the vibration control problem for a stable inverted pendulum with passive mass–spring-pendulum-type DVA is investigated. The equation of motion is expressed in the dimensionless form. The equivalent mass ratio is established and shows that effect of DVA is proportional to the square of distance from DVA to the center of oscillation. In practice, the distance between DVA and center of oscillation in

inverted-pendulum case is larger than the distance in conventional pendulum case. Parameters of DVA are chosen by maximizing the damping characteristic of the system. By using the concept of equivalent mass or damping ratio, the location where DVA has no effect is showed. Numerical simulation is done for an example of the articulated tower in the ocean. In the example, to reduce the vibration of main structure, conventional mass–spring-pendulum-type DVA requires a long pendulum arm. To address the problem, mass–spring inverted-pendulum-type DVA is considered and good effect is obtained.

2. Equation of motion

2.1. Mass–spring-pendulum-type DVA

As shown in Fig. 1, inverted-pendulum structure has a concentrated mass m at the top and one degree of freedom θ about z-axis.

The concentrated mass is supported by a beam. We consider the case where the beam-bending stiffness is large enough so that the beam can be modeled as a rigid rod which has length l and uniform mass per unit length ρ. The viscous structural damping constant is denoted by C_s. To keep the structure in a stable upright position, a restoring moment is produced by a torsion spring with spring constant K. The dynamic absorber has mass–spring-pendulum type with mass m_d, length l_d, spring constant k_d, and damping constant c_d. DVA is attached to the structure through a differential pulley mechanism to eliminate the geometric nonlinearity of spring and damping device. Similar mechanism has been proposed in Ref. [28]. The pulley's radius is assumed as r. Strings and pulley do not have slip. Denote the angular variation of the dynamic absorber with respect to the main structure as θ_d. Taking the coordinate system as shown in Fig. 1, the positions of the structure (x,y) and the dynamic absorber (x_d, y_d) is obtained easily:

$$x = l\sin\theta, \quad y = l\cos\theta,$$
$$x_d = l_d\sin(\theta_d - \theta) + d\sin\theta, \quad y_d = d\cos\theta - l_d\cos(\theta_d - \theta). \tag{1}$$

To obtain the kinetic energy and potential energy of the supported rod, consider its elemental length ds, which is located at distance of s from the rotating point. Position and the mass of the elemental length ds are, respectively,

$$x_b(s) = s\sin\theta, \quad y_b(s) = s\cos\theta, \quad \mathrm{d}m_b = \rho\,\mathrm{d}s. \tag{2}$$

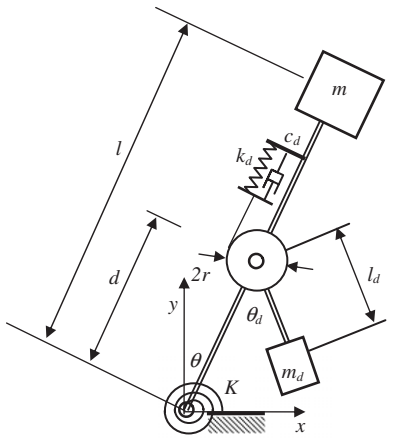

Fig. 1. Inverted-pendulum structure with mass–spring-pendulum absorber.

Kinetic energy K_E, potential energy P_E and dissipative energy D_E are expressed as follows:

$$K_E = \frac{1}{2}m(\dot{x}^2+\dot{y}^2)+\frac{1}{2}m_d(\dot{x}_d^2+\dot{y}_d^2)+\frac{1}{2}\int_0^l[(\dot{x}_b(s))^2+(\dot{y}_b(s))^2]\rho\,\mathrm{d}s$$
$$= \frac{1}{2}\left(ml^2\dot{\theta}^2+m_dd^2\dot{\theta}^2+m_dl_d^2(\dot{\theta}-\dot{\theta}_d)^2+2m_ddl_d\dot{\theta}(\dot{\theta}_d-\dot{\theta})\cos\,\theta_d+\frac{1}{3}\rho l^3\dot{\theta}^2\right), \tag{3}$$

$$P_E = mgy+m_dgy_d+\frac{K\theta^2+k_d(r\theta_d)^2}{2}+\int_0^l\rho gy_b(s)\,\mathrm{d}s$$
$$= \frac{1}{2}(K\theta^2+k_dr^2\theta_d^2+(2ml+2m_dd+\rho l^2)g\cos\,\theta-2m_dl_dg\cos(\theta-\theta_d)), \tag{4}$$

$$D_E = C_s\dot{\theta}^2+c_d(r\dot{\theta}_d)^2. \tag{5}$$

When the structure is excited by external moment $M(t)$, the equations of motion of the inverted-pendulum DVA are derived using Lagrange's equations:

$$\frac{\mathrm{d}}{\mathrm{d}t}\left(\frac{\partial K_E}{\partial\theta}\right)-\frac{\partial K_E}{\partial\theta}+\frac{\partial P_E}{\partial\theta}+\frac{\partial D_E}{\partial\dot{\theta}}=M(t), \tag{6}$$

$$\frac{\mathrm{d}}{\mathrm{d}t}\left(\frac{\partial K_E}{\partial\dot{\theta}_d}\right)-\frac{\partial K_E}{\partial\theta_d}+\frac{\partial P_E}{\partial\theta_d}+\frac{\partial D_E}{\partial\dot{\theta}_d}=0. \tag{7}$$

Substituting Eqs. (3)–(5) in Eqs. (6)–(7) results in

$$ml^2\ddot{\theta}+\frac{\rho l^3}{3}\ddot{\theta}-m_dl_d^2\ddot{\theta}_d+m_d(d^2+l_d^2)\ddot{\theta}+m_ddl_d\cos\,\theta_d(\ddot{\theta}_d-2\ddot{\theta})+m_ddl_d(2\dot{\theta}-\dot{\theta}_d)\dot{\theta}_d\sin\,\theta_d+C_s\dot{\theta}+K\theta$$
$$-\left(ml+m_dd+\frac{\rho l^2}{2}\right)g\sin\,\theta+m_dl_dg\sin(\theta-\theta_d)=M(t), \tag{8}$$

$$(m_ddl_d\cos\,\theta_d-m_dl_d^2)\ddot{\theta}+m_dl_d^2\ddot{\theta}_d+k_dr^2\theta_d-m_dl_dd\dot{\theta}^2\sin\,\theta_d-m_dl_dg\sin(\theta-\theta_d)+c_dr^2\dot{\theta}_d=0. \tag{9}$$

The governing equations (8) and (9) are used in the numerical calculation. However, in order to determine DVA's parameters, governing equations are linearized and the structural damping is ignored. This implies that DVA is only designed to reduce the undamped vibration of the tower in the linear case. The effect of DVA in the nonlinear case must be checked by numerical calculation. Neglecting the terms of higher power and ignoring structural damping, linearized equations corresponding to Eqs. (8) and (9) can be rewritten in the matrix form:

$$\begin{bmatrix} ml^2+\frac{\rho l^3}{3}+m_d(d-l_d)^2 & m_ddl_d-m_dl_d^2 \\ m_ddl_d-m_dl_d^2 & m_dl_d^2 \end{bmatrix}\begin{bmatrix}\ddot{\theta}\\ \ddot{\theta}_d\end{bmatrix}+\begin{bmatrix}0 & 0\\ 0 & c_dr^2\end{bmatrix}\begin{bmatrix}\dot{\theta}\\ \dot{\theta}_d\end{bmatrix}$$
$$+\begin{bmatrix} K-mgl-\frac{\rho gl^2}{2}-m_dg(d-l_d) & -m_dgl_d \\ -m_dgl_d & k_dr^2+m_dgl_d\end{bmatrix}\begin{bmatrix}\theta\\ \theta_d\end{bmatrix}=\begin{bmatrix}M(t)\\ 0\end{bmatrix}. \tag{10}$$

Introducing the dimensionless parameters

$$\mu=\frac{m_d}{m+\rho l/3},\quad \gamma=\frac{d-l_d}{l},$$
$$\omega_s=\sqrt{\frac{K}{ml^2+\rho l^3/3}-\frac{(6m+3\rho l)g}{6ml+2\rho l^2}}=\sqrt{\frac{6K-gl(6m+3\rho l)}{2l^2(3m+\rho l)}},$$
$$\omega_d=\sqrt{\frac{k_dr^2}{m_dl_d^2}+\frac{g}{l_d}},\quad \xi=\frac{c_dr^2}{2m_d\omega_dl_d^2},\quad \alpha=\frac{\omega_d}{\omega_s},\quad \eta=\frac{g}{\omega_s^2l}, \tag{11}$$

where μ is the mass ratio, γ specifies the position of the dynamic absorber, ω_s is natural frequency of the structure, ω_d and ξ are atural frequency and damping ratio of DVA, respectively, α is natural frequency ratio, η specifies the distribution of mass of the structure, and further defining

$$u = l\theta, \quad u_d = l_d\theta_d. \tag{12}$$

Eq. (10) can be rewritten in the dimensionless form:

$$\begin{bmatrix} 1+\mu\gamma^2 & \mu\gamma \\ \mu\gamma & \mu \end{bmatrix} \begin{bmatrix} \ddot{u} \\ \ddot{u}_d \end{bmatrix} + \omega_s \begin{bmatrix} 0 & 0 \\ 0 & 2\xi\alpha\mu \end{bmatrix} \begin{bmatrix} \dot{u} \\ \dot{u}_d \end{bmatrix} + \omega_s^2 \begin{bmatrix} 1-\mu\gamma\eta & -\mu\eta \\ -\mu\eta & \mu\alpha^2 \end{bmatrix} \begin{bmatrix} u \\ u_d \end{bmatrix} = \begin{bmatrix} \frac{3M(t)}{3ml+\rho l^2} \\ 0 \end{bmatrix}. \tag{13}$$

Matrix equation (13) can be used in the design of DVA.

2.2. Mass–spring inverted-pendulum dynamic absorber

In many cases, required length of dynamic absorber in Fig. 1 is too long because of the long period of the structure. The mass–spring inverted-pendulum type dynamic absorber as shown in Fig. 2 can solve this problem. The structure in Fig. 2 is similar to that of Fig. 1, but the absorber is inverted. Suppose that the supported rod for DVA mass m_d can be neglected. The motion equations in this case are obtained from Eqs. (8) and (9) by replacing l_d with $-l_d$.

As seen from Eq. (11) natural frequency ω_d of absorber can be reduced without increasing length l_d.

3. Stability analysis

3.1. Linear analysis

The stability analysis in the linear case focuses on the linearized dimensionless Eq. (13). There are some stability criteria. We use here the stability criterion according to Lyapunov matrix equation. The criterion is given by the following conditions:

- Damping matrix is a symmetric positive-semi-definite matrix;
- Stiffness matrix is a symmetric positive-definite matrix.

Using the matrices in Eq. (13) one obtains the stability condition:

$$\begin{cases} 1-\mu\gamma\eta > 0, \\ (1-\mu\gamma\eta)\mu\alpha^2 - \mu^2\eta^2 > 0. \end{cases} \tag{14}$$

Because $\mu > 0$, the stability condition is reduced to

$$(1-\mu\gamma\eta)\alpha^2 - \mu\eta^2 > 0. \tag{15}$$

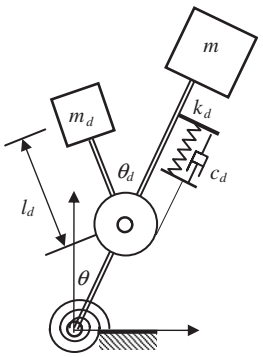

Fig. 2. Inverted-pendulum structure with mass–spring inverted-pendulum absorber.

Stability condition (15) gives limit values for system parameters. For example, if position of absorber is too high (γ too large), structure–absorber system will be unstable.

3.2. Nonlinear analysis

The above analytical investigations of motion stability often focus on local solution regions surrounding equilibrium or critical points. These results are applicable to small perturbations case, in which the linear approximation is suitable. Global analysis, or analysis of large-amplitude motions, is usually studied by numerical methods. One of the effective ways is Hsu's cell-to-cell mapping method [29]. This method divides the operating domain of the nonlinear system into a large number of smaller regions or "cells". The trajectories from one cell to another create a so-called cell-to-cell map. This map shows the cells that have a high probability of moving into the equilibrium point. Some fundamental concepts and properties of the cell-to-cell mapping method are briefly discussed below. Fig. 3 illustrates a two-dimensional grid of cells that might be used to create a cell-to-cell map.

The state space is divided into four rectangular cells. Some trajectories are computed for each cell. The trajectory begins at a point within the cell and ends after a specified time period. The association between the starting cell and the endpoint cell determines one element of the cell-to-cell map. The illustration is seen from Fig. 3, where two trajectories are shown starting from within each cell. The cell-to-cell map Φ for the system in Fig. 3 would be represented numerically by a four-by-four matrix, whose columns and rows represent the endpoint cells and the starting cells, respectively. The cell map can be interpreted in a probabilistic sense. For example, if the initial condition of the nonlinear system is located within cell 3, then Fig. 3 shows that the solution at the next time step will lie in cell 2 with probability 1/2 and in cell 4 with probability 1/2. Using this probabilistic interpreter for other cells, we obtain the cell map Φ as

$$\Phi = \begin{bmatrix} 0 & 0 & 0 & 0 \\ 1/2 & 1 & 1/2 & 0 \\ 0 & 0 & 0 & 0 \\ 0 & 0 & 1/2 & 0 \end{bmatrix}$$

The evolution of the cell-to-cell mapping as time increases is specified by the probability vector p. The number of elements in p will be equal to the number of cells in the cell-to-cell map and the numerical value of an element in p is defined as the probability that a solution of the nonlinear system lies within the associated domain cell. The probability vector p representing the system in Fig. 3 has the form

$$p(0) = \begin{bmatrix} 1/4 & 1/4 & 1/4 & 1/4 \end{bmatrix}^{\mathrm{T}}, \quad p(1) = \begin{bmatrix} 0 & 1/2 & 0 & 1/8 \end{bmatrix}^{\mathrm{T}},$$

$$p(2) = p(3) = \cdots = p(\infty) = \begin{bmatrix} 0 & 1/2 & 0 & 0 \end{bmatrix}^{\mathrm{T}}.$$

It shows that after two steps, four trajectories (a half of the initial trajectories) lie in cell 2 and four remaining trajectories leave the cell domain. The probability vector has the following property:

$$p(k+1) = \Phi p(k). \tag{16}$$

The one-step index represents a time increment of the specified time period of each trajectory. Hsu devised two important concepts called absorbing cells and transient cells. A *transient cell* has the property that once a

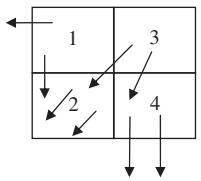

Fig. 3. An example of the cell mapping.

solution leaves the cell, it does not return. An *absorbing cell* has the property that once a solution enters the cell, it does not leave. Therefore, only the absorbing cell has the steady-state probability vector. From Eq. (16), one can see that the steady-state probability vector p^* will satisfy

$$p^* = \Phi p^* \Leftrightarrow (I - \Phi)p^* = 0. \tag{17}$$

Eq. (17) shows that p^* must be an eigenvector of cell-to-cell map matrix Φ. These special eigenvectors are associated with eigenvalues equal to unity. The non-zero elements of p^* point to the absorbing cells in the map. Once the absorbing cells have been found, probability vector can be sorted into absorbing and transient cells. Let p_a represent probability vector elements associated with absorbing cells and let p_t represent those associated with transient cells. Eq. (17) can then be written in the following form:

$$\begin{bmatrix} p_a(k+1) \\ p_t(k+1) \end{bmatrix} = \begin{bmatrix} \Phi_{aa} & \Phi_{at} \\ 0 & \Phi_{tt} \end{bmatrix} \begin{bmatrix} p_a(k) \\ p_t(k) \end{bmatrix}. \tag{18}$$

The solution is

$$p_a(k+1) = \Phi_{aa} p_a(k) + \Phi_{at}(\Phi_{tt})^k p_t(0). \tag{19}$$

Recall that the unit-amplitude eigenvalues of Φ serve to locate the absorbing cells. Therefore, Φaa will contain unit-amplitude eigenvalues and the remaining eigenvalues, which are also the eigenvalues of Φtt, will have amplitude less than unity. From Eq. (19) we see that when $k \to \infty$, $(\Phi_{tt})^k \to 0$ and trajectories starting from transient cells will pass into the absorbing cells. The probability that a solution starting in a transient cell will eventually pass into an absorbing cell is defined by the matrix

$$R = \sum_{k=0}^{\infty} \Phi_{at}(\Phi_{tt})^k = \Phi_{at}(I - \Phi_{tt})^{-1}. \tag{20}$$

The (i, j) element of R represents the probability for solutions from transient cell j to pass into absorbing cell i. The list of transient cells that have a high probability of moving into an absorbing cell determines the *basin of attraction* for the absorbing cell. In summary, the cell-to-cell mapping method in this paper contains the following step:

- *Step* 1: Divide the domain of interest into cells.
- *Step* 2: Compute the cell-to-cell map matrix Φ by solving a series of nonlinear system equation. Entry Φ_{ji} is the number of trajectories that end in cell j divided by the total number of trajectories that were started from cell i.
- *Step* 3: Find the unit-amplitude eigenvalues of Φ, as well as their associated eigenvectors p^*. The non-zero elements of p^* point to the absorbing cells.
- *Step* 4: Sort the probability cell vector such that Φ is decomposed into the form of Eq. (18). This manipulation defines Φ_{at} and Φ_{tt}.
- *Step* 5: Compute the absorption matrix R using Eq. (20) to determine the basin of attraction for the absorbing cell.

4. Equivalent mass ratio

Efficiency of DVA depends on parameters of the primary system and DVA itself. When parameters of the primary system and mass ratio μ are fixed, efficiency of DVA can be defined by the equivalent mass ratio as follows. Let

$$M(t) = A \sin \omega t, \quad u(t) = U \sin \omega t, \quad u_d(t) = U_d \sin \omega t. \tag{21}$$

Substituting Eq. (21) into Eq. (13) and neglecting damping term yields

$$-\omega^2 \begin{bmatrix} 1 + \mu\gamma^2 & \mu\gamma \\ \mu\gamma & \mu \end{bmatrix} \begin{bmatrix} U \\ U_d \end{bmatrix} + \omega_s^2 \begin{bmatrix} 1 - \mu\gamma\eta & -\mu\eta \\ -\mu\eta & \mu\alpha^2 \end{bmatrix} \begin{bmatrix} U \\ U_d \end{bmatrix} = \begin{bmatrix} \frac{3A}{3ml + \rho l^2} \\ 0 \end{bmatrix}. \tag{22}$$

One gets from Eq. (22)

$$\begin{bmatrix} U \\ U_d \end{bmatrix} = \begin{bmatrix} \frac{3A}{3ml+\rho l^2}\frac{(\alpha^2\omega_s^2-\omega^2)}{D} \\ \frac{3A}{3ml+\rho l^2}\frac{(\gamma\omega^2+\eta\omega_s^2)}{D} \end{bmatrix}, \quad D = \omega_s^2\omega_d^2\left[\left(1-\frac{\omega^2}{\omega_s^2}\right)\left(1-\frac{\omega^2}{\omega_d^2}\right)-\mu\left(\eta+\gamma\frac{\omega^2}{\omega_s^2}\right)\left(\gamma+\eta\frac{\omega^2}{\omega_s^2}\right)\right]. \tag{23}$$

The purpose of the absorber is to reduce the large peak of resonant vibration at ω_s. Therefore, natural frequency of absorber is tuned to be the similar frequency. In the resonant frequency domain one has $\omega \approx \omega_s \approx \omega_d$. Thus from Eq. (23) we obtain

$$D \approx \omega_s^2\omega_d^2\mu(\eta+\gamma)^2 = \omega_s^2\omega_d^2\mu_e, \tag{24}$$

where equivalent mass ratio is defined by

$$\mu_e = \mu(\eta+\gamma)^2. \tag{25}$$

Efficiency of DVA depends on the term$\gamma+\eta$. Using Eq. (11), one gets

$$\gamma+\eta = \frac{d-l_d}{l}+\frac{g}{\omega_s^2 l} = \frac{d-l_d+l_e}{l}, \tag{26}$$

where equivalent length of pendulum is defined by

$$l_e = \frac{g}{\omega_s^2} = \frac{2gl^2(3m+\rho l)m_d}{6K-gl(6m+3\rho l)}. \tag{27}$$

It is clearly seen from Eq. (26) that the location of DVA, namely, $d-l_d$ is an important factor and the larger the $d-l_d$, better the efficiency of DVA. When the location of absorber on an inverted pendulum is above the fulcrum, $d-l_d>0$. In a case of normal pendulum with the absorber which is located below the fulcrum, $d-l_d<0$. Therefore, it can be concluded that the performance of DVA on an inverted pendulum is better than on a normal pendulum system.

5. Optimal tuning for free vibration

As mentioned in Introduction, the concepts for designing DVA are several. Here, the idea is to improve the damping characteristic of the primary system using DVA [4–6]. The characteristic polynomial corresponding to Eq. (13) is given by

$$P(\lambda) = \mathrm{Det}\left(\lambda^2\begin{bmatrix} 1+\mu\gamma^2 & \mu\gamma \\ \mu\gamma & \mu \end{bmatrix} + \lambda\omega_s\begin{bmatrix} 0 & 0 \\ 0 & 2\xi\alpha\mu \end{bmatrix} + \omega_s^2\begin{bmatrix} 1-\mu\gamma\eta & -\mu\eta \\ -\mu\eta & \mu\alpha^2 \end{bmatrix}\right), \tag{28}$$

or

$$P(\lambda) = a_4\lambda^4 + a_3\lambda^3 + a_2\lambda^2 + a_1\lambda + a_0, \tag{29}$$

where

$$\begin{aligned} &a_4 = 1; \quad a_3 = 2\alpha(1+\gamma^2\mu)\xi\omega_s, \quad a_2 = (1+\alpha^2+\alpha^2\gamma^2\mu+\gamma\eta\mu)\omega_s^2, \\ &a_1 = 2\alpha\xi\omega_s^3(1-\gamma\eta\mu), \quad a_0 = \omega_s^4(\alpha^2-\eta^2\mu-\eta\alpha^2\gamma\mu). \end{aligned} \tag{30}$$

The roots of the polynomial $P(\lambda)$ are called the poles of system (structure and absorber). If the system is stable, these poles must have negative real parts, i.e. must lie in the left half of the complex plane. It is known that the real parts of the poles show the attenuation of the system response and the imaginary parts of the poles show the number of oscillation cycles. Therefore, the magnitudes of the real parts should be as large as possible and the magnitudes of the imaginary parts should be as small as possible. We will show that the case corresponding to four repeated negative real poles is optimal. This optimal design is carried out in 3 steps. Firstly, the DVA's spring constant is tuned to make the repeated real parts. Secondly, DVA's damping constant is tuned to make the repeated magnitudes of imaginary parts. Lastly, the other DVA's parameters are

tuned to make the imaginary parts zero. The mathematical explanation of the optimal design is presented below. Denoting the roots of $P(\lambda)$ by λ_i $(i = 1,\ldots,4)$, which can be real or complex. In any case, we have

$$-\sum_{i=1}^{4} \mathrm{Re}(\lambda_i) = a_3 = 2\alpha(1+\gamma^2\mu)\xi\omega_s, \tag{31}$$

$$\Rightarrow \min_{i=1,..4}(|\mathrm{Re}(\lambda_i)|) \leqslant \frac{\alpha(1+\gamma^2\mu)\xi\omega_s}{2}. \tag{32}$$

Considering Eq. (11), we can see that the right-hand side of Eq. (32) does not depend on DVA's spring constant k_d. Since we want real parts large, in the first step, DVA's spring constant is tuned to make Eq. (32) become an equality. This means that all real parts of poles have the same value. We denote the repeated real part by δ_0. In this case, the system poles are 2 complex conjugate pairs. We denote these poles by $\delta_0 \pm \mathrm{i}\delta_1$ and $\delta_0 \pm \mathrm{i}\delta_2$, where δ_1 and δ_2 are corresponding imaginary parts. After tuning to the repeated real parts case, we will show that DVA's damping constant c_d should be tuned to equalize the imaginary parts δ_1 and δ_2. We have

$$P(\lambda) = ((\lambda-\delta_0)^2+\delta_1^2)((\lambda-\delta_0)^2+\delta_2^2). \tag{33}$$

Comparing Eqs. (29) and (33), using Eq. (30) yields

$$-4\delta_0 = 2\alpha(1+\gamma^2\mu)\xi\omega_s, \tag{34}$$

$$6\delta_0^2+\delta_1^2+\delta_2^2 = (1+\alpha^2+\alpha^2\gamma^2\mu+\gamma\eta\mu)\omega_s^2, \tag{35}$$

$$-4\delta_0^3 - 2\delta_0(\delta_1^2+\delta_2^2) = 2\alpha\xi\omega_s^3(1-\gamma\eta\mu). \tag{36}$$

$$(\delta_0^2+\delta_1^2)(\delta_0^2+\delta_2^2) = \omega_s^4(\alpha^2-\eta^2\mu-\eta\alpha^2\gamma\mu) \tag{37}$$

Eliminating ξ, α and δ_0 from Eqs. (34)–(37), we obtain the relation between imaginary parts δ_1 and δ_2:

$$\frac{6\frac{\omega_s^2(1-\gamma\eta\mu)}{(1+\gamma^2\mu)} - 2(\delta_1^2+\delta_2^2) - (1+\gamma\eta\mu)\omega_s^2}{\left(\frac{\omega_s^2(1-\gamma\eta\mu)}{(1+\gamma^2\mu)}+\frac{\delta_1^2-\delta_2^2}{2}\right)\left(\frac{\omega_s^2(1-\gamma\eta\mu)}{(1+\gamma^2\mu)}+\frac{\delta_2^2-\delta_1^2}{2}\right)+\eta^2\mu\omega_s^4} = \frac{(1+\gamma^2\mu)}{(1-\eta\gamma\mu)\omega_s^2}. \tag{38}$$

By using an evident inequality

$$\left(\frac{\omega_s^2(1-\gamma\eta\mu)}{(1+\gamma^2\mu)}+\frac{\delta_1^2-\delta_2^2}{2}\right)\left(\frac{\omega_s^2(1-\gamma\eta\mu)}{(1+\gamma^2\mu)}+\frac{\delta_2^2-\delta_1^2}{2}\right) \leqslant \left[\frac{\omega_s^2(1-\gamma\eta\mu)}{(1+\gamma^2\mu)}\right]^2 \tag{39}$$

after some manipulation from Eq. (38), we obtain

$$\delta_1^2+\delta_2^2 \geqslant \frac{4(1-\gamma\eta\mu)^2-\mu(\eta+\gamma)^2}{2(1+\gamma^2\mu)(1-\gamma\eta\mu)}\omega_s^2, \tag{40}$$

$$\Rightarrow \max_{i=1,2}(\delta_i^2) \geqslant \frac{4(1-\gamma\eta\mu)^2-\mu(\eta+\gamma)^2}{4(1+\gamma^2\mu)(1-\gamma\eta\mu)}\omega_s^2. \tag{41}$$

The right-hand side of Eq. (41) does not depend on DVA's damping constant c_d. Since we want magnitudes of imaginary parts to be small, in the second step, DVA's damping constant is tuned to make Eq. (41) become an equality, i.e. $\delta_1 = \delta_2$.

$$\delta_1 = \delta_2 = \omega_s\sqrt{\frac{4(1-\gamma\eta\mu)^2-\mu(\eta+\gamma)^2}{4(1+\gamma^2\mu)(1-\gamma\eta\mu)}}. \tag{42}$$

To make δ_1 and δ_2 real, we need

$$2(1-\gamma\eta\mu) \geqslant \sqrt{\mu}|\eta+\gamma|. \tag{43}$$

In the last step, the remaining DVA's parameters μ and γ should be chosen to make $\delta_1 = \delta_2 = 0$. This means inequality (43) becomes an equality. However, in most of the practical applications, we have $\mu < 5\%$, $|\gamma| < 1$, and $(1-\gamma\eta\mu)$ must be large enough due to stability condition, then $2(1-\gamma\eta\mu) \gg \sqrt{\mu}|\eta+\gamma|$. Therefore, in most cases, the last step of the optimal design could not be carried out. In summary, we only achieve the repeated complex poles case, not the repeated real poles case. Substituting Eq. (42) in Eqs. (34)–(37), we obtain the real part δ_0, optimal DVA's damping ratio ξ_{opt} and optimal DVA's frequency ratio α_{opt}:

$$\alpha_{\text{opt}} = \frac{\sqrt{(1-\gamma\eta\mu)^2 + \mu\eta^2(1+\gamma^2\mu)^2}}{(1+\gamma^2\mu)\sqrt{1-\gamma\eta\mu}}, \tag{44}$$

$$\xi_{\text{opt}} = \frac{\sqrt{\mu(\gamma+\eta)^2}}{\sqrt{(1+\gamma^2\mu)[(1-\gamma\eta\mu)^2 + \mu\eta^2(1+\gamma^2\mu)^2]}}, \tag{45}$$

$$\delta_0 = -\frac{\omega_s}{2}\sqrt{\frac{\mu(\gamma+\eta)^2}{(1-\gamma\eta\mu)(1+\gamma^2\mu)}}. \tag{46}$$

We also note that stability condition (15) is satisfied with the solution (44) as

$$(1-\mu\gamma\eta)\alpha^2 - \mu\eta^2 = \frac{(1-\gamma\eta\mu)^2 + \mu\eta^2(1+\gamma^2\mu)^2}{(1+\gamma^2\mu)^2} - \mu\eta^2 = \frac{(1-\gamma\eta\mu)^2}{(1+\gamma^2\mu)^2} > 0. \tag{47}$$

In the optimal condition case, as described, all four system-damping ratios have the same value:

$$\xi_i = -\frac{\text{Re}\lambda_i}{|\lambda_i|} = \frac{-\delta_0}{\sqrt{\delta_0^2+\delta_1^2}} = \frac{-\delta_0}{\sqrt{\delta_0^2+\delta_2^2}} = \frac{\sqrt{\mu(\gamma+\eta)^2}}{2(1-\mu\gamma\eta)} \quad (i = 1,\ldots,4). \tag{48}$$

As discussed above, we have $2(1-\gamma\eta\mu) \gg \sqrt{\mu}|\eta+\gamma|$. Then the damping ratio is less than 1 in most cases. Using Eqs. (27), (26) and (11), we express the damping ratio by the physical variables

$$\xi_i = \frac{\sqrt{\mu l^2(d-l_d+l_e)^2}}{2(l^2-\mu l_e(d-l_d))} \quad (i = 1,\ldots 4). \tag{49}$$

It is seen from Eq. (48) (and also from Eq. (25)) that when γ is equal to $-\eta$, absorber has no effect. This situation is explained as follows. At the special point, where γ is equal to $-\eta$, the inertial force and the gravity force acting on DVA are balanced. So the vibration of the structures does not excite the DVA and, conversely, DVA does not excite or mitigate the vibration of structure either. This can be seen from the second equation of Eq. (13). The inertial force acting on the absorber is $\mu\gamma\ddot{u}$ and the gravity force is $-\omega_s^2\mu\eta u$. When the main structure vibration has frequency ω_s, we have $\ddot{u} = -\omega_s^2 u$. The total external force acting on the absorbers is $-\mu\omega_s^2 u(\gamma+\eta)$. At the location, where $\gamma+\eta = 0$, no force acts on the mass of the absorber. Relative displacement between absorber and structure cannot be maintained and absorber does not work at all at the resonant frequency ω_s. From Eqs. (25) and (26), it can be seen that the effect of absorber is proportional to the square of distance of the absorber from the center of oscillation. This special effect was indicated in the theory of location [7], which is presented in Introduction

6. Example

One of the examples of inverted pendulum is the articulated tower in the ocean. Compliant platforms such as articulated towers are economically attractive for deep-water conditions because of their reduced structural weight compared to conventional platforms. The foundation of the tower does not resist lateral forces due to wind, waves and currents; instead, restoring moments are provided by a large buoyancy force. The environmental loadings, e.g. wind and wave, may occur or stop at random. Thus, DVA can be installed in the

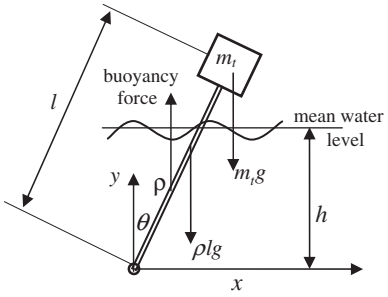

Fig. 4. Model of the articulated tower.

articulated tower to increase the damping characteristic. Consider an articulated tower as shown in Fig. 4. The figure consists of a tower submerged in the ocean having a concentrated mass m_t at the top. Assuming that the tower stiffness is infinite ($EI = \infty$), the friction in the pivot is ignored. The tower has a uniform mass per unit length ρ, length l and diameter D. Tower diameter is much smaller than its length ($D \ll l$). End mass m_t is considered to be concentrated at the end of the tower.

Using stability condition (13), one can check if the structure is statically stable or not. It is seen from Fig. 4 that restoring moment M_b produced by buoyancy force is determined by

$$M_b = \rho_w g \frac{\pi D^2}{4} \frac{l_s^2}{2} \sin\,\theta, \tag{50}$$

where ρ_w is mass density of fluid and l_s is length of the submerged part of the tower. Considering that θ is small, length l_s is approximated by height elevation h and $\sin\theta \approx \theta$. From Eq. (50), it is easy to find the spring constant of the equivalent torsion spring:

$$K = \tfrac{1}{8}\pi \rho_w g h^2 D^2. \tag{51}$$

We use the following numerical data [24]: tower length $l = 400\,\text{m}$, tower diameter $D = 15\,\text{m}$, tower uniform mass per unit length $\rho_r = 20 \times 10^3\,\text{kg/m}$, end mass $m_t = 2.5 \times 10^5\,\text{kg}$, mean water level $h = 350\,\text{m}$, water density $\rho_w = 1025\,\text{kg/m}^3$, structural damping is 2%. Equivalent torsion spring constant is calculated from (51):

$$K = 1.1 \times 10^{11}\,\text{Nm}, \tag{52}$$

Natural frequency of the tower is calculated from (11):

$$\omega_s = \sqrt{\frac{6K - gl(6m + 3\rho l)}{2l^2(3m + \rho l)}} = 0.44\,\text{rad/s}. \tag{53}$$

To reduce the vibration of the tower, a dynamic absorber is proposed to be installed inside the box of the tower's column. If the mass–spring-pendulum-type absorber is used, the required length of pendulum is too long (about 50 m) because of the long period of the tower. So, mass–spring inverted-pendulum-type absorber is used as shown in Fig. 5.

Assuming that absorber's mass is about $5.8 \times 10^4\,\text{kg}$ ($\mu = 2\%$), length of absorber l_d is fixed at 15 m, absorber is located at distance $d = 350\,\text{m}$ from the seabed, pulley's radius r is taken 2 m. Parameters of the DVA are obtained by the method discussed in Section 5. From Eqs. (44) and (45), one obtains 2 dimensionless parameters of the absorber:

$$\alpha_{\text{opt}} = 0.983, \quad \xi_{\text{opt}} = 0.145. \tag{54}$$

Physical parameters of DVA are obtained from Eq. (11). Because absorber has inverted pendulum type, we must replace l_d with $-l_d$ in all expressions. We have

$$k_d = m_d\left(\alpha_{\text{opt}}^2 \omega_s^2 + \frac{g}{l_d}\right)\frac{l_d^2}{r^2} = 2.75 \times 10^6\,\text{N/m}, \quad c_d = 2\xi_{\text{opt}} m_d \alpha_{\text{opt}} \omega_s \frac{l_d^2}{r^2} = 4.14 \times 10^5\,\text{Ns/m}. \tag{55}$$

As seen from Eq. (47), linearized system is stable. Large amplitude motions are analyzed by cell-to-cell mapping method as discussed in Section 3. The motion equations (8) and (9) require four-dimensional state space domain. The domain of interest is selected such that $|\theta| < \theta_{\max} = 0.03$ rad, $|\dot{\theta}| < \omega_s \theta_{max}$, $|\theta_d| < \theta_{d\max} = \pi/6$ rad, $|\dot{\theta}_d| < \omega_s \theta_{dmax}$. The selected domain covers the maximum tower response, 5×10^{-3} rad, due to significant wave height of 15 m [24]. The complete four-dimensional cell map, however, takes much memory and time to create. The high-dimensional cell map also leads to difficulty in the eigenvalues calculation and in results visualization. The most common approach is to reduce state variables of interest. In this paper, we consider two variables describing the motion of structure such as θ and $\dot{\theta}$. Therefore, the state space domain is divided such that, two dimensions of variables θ and $\dot{\theta}$ have 21 divisions and two remaining dimensions of variables θ_d and $\dot{\theta}_d$ have only 1 division. One hundred trajectories are started from each domain cell. The nonlinear motion equations are solved 44,100 times in total. Each trajectory was followed for 15 s. Because only two variables θ and $\dot{\theta}$ are considered, the initial conditions of θ and $\dot{\theta}$ are generated randomly in each domain cell and the initial conditions of θ_d and $\dot{\theta}_d$ are fixed.

The first set of DVA's initial conditions is chosen as $\theta_d(0) = 0$ and $\dot{\theta}_d(0) = 0$. This set has the effect of forcing DVA to have no initial relative motion with respect to the structure. A second set of DVA's initial conditions is chosen as $\theta_d(0) = -\theta(0)$ and $\dot{\theta}_d(0) = -\dot{\theta}(0)$. This set has the effect of forcing DVA to stay at equilibrium position at the beginning of each trajectory. Fig. 6 shows the probability of absorption into the absorbing cell, which is located on the equilibrium point. The results are similar in two cases. In the figure, a dark-shaded transient cell indicates a higher probability of being absorbed. The darkest region, therefore, describes the basin of attraction. We can see that the motion trajectories of the combined system (structure and DVA) might leave the domain considered if the initial deflection of structure exceeds 0.01 rad or the initial angular velocity of structure exceeds 5×10^{-3} rad/s.

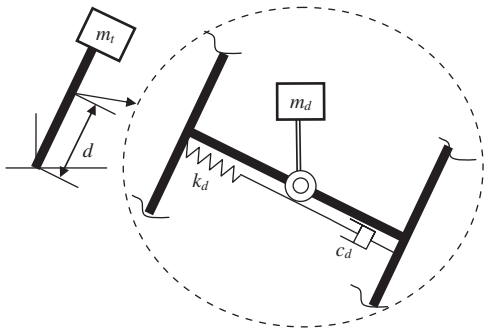

Fig. 5. Mass–spring absorber locates inside the column box.

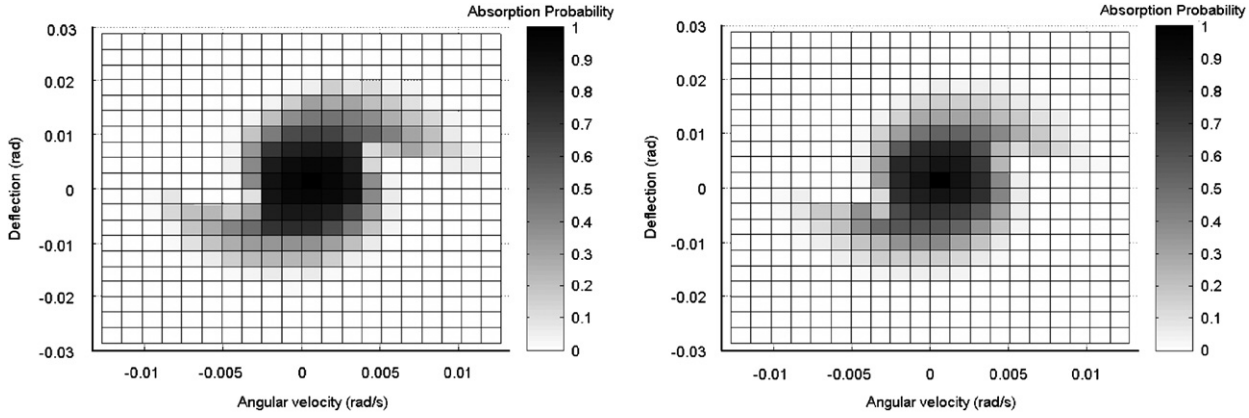

Fig. 6. Absorption probability for equilibrium point in the case of $\theta_d(0) = 0, \dot{\theta}_d(0) = 0$ (left) and in the case of $\theta_d(0) = -\theta$ (0), $\dot{\theta}_d(0) = -\dot{\theta}(0)$ (right).

Figs. 7 and 8 show the time response of the tower's deflection and the absorber's deflection induced by the initial velocities of 1.5×10^{-3} and 3×10^{-3} rad/s.

It can be seen that, large initial velocity leads to nonlinearity of DVA and decreases effect of DVA. The forced response of the tower is often induced by wave load. However, calculations of wave load are

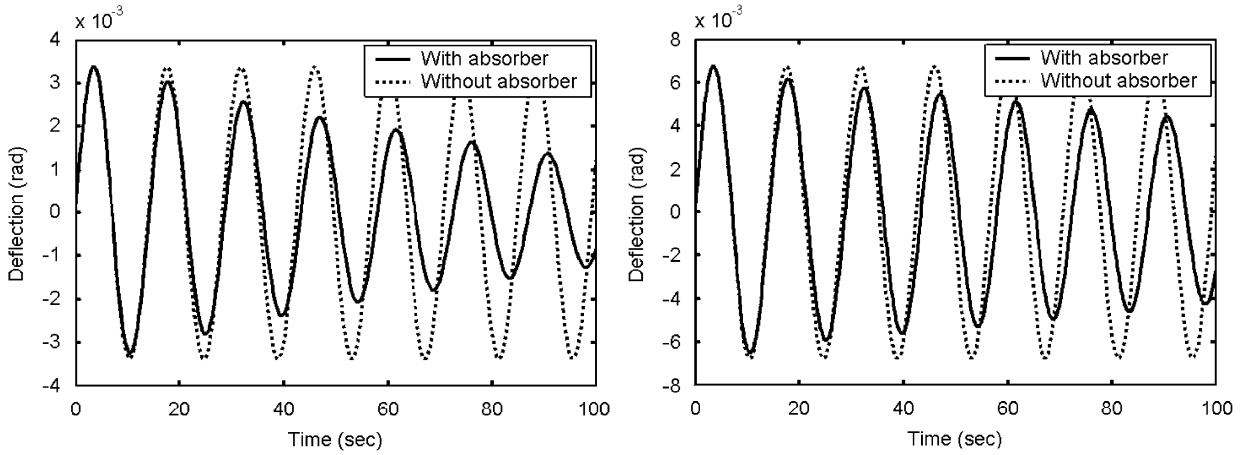

Fig. 7. Time response of the tower with initial velocity 1.5×10^{-3} rad/s (left) and 3×10^{-3} rad/s (right).

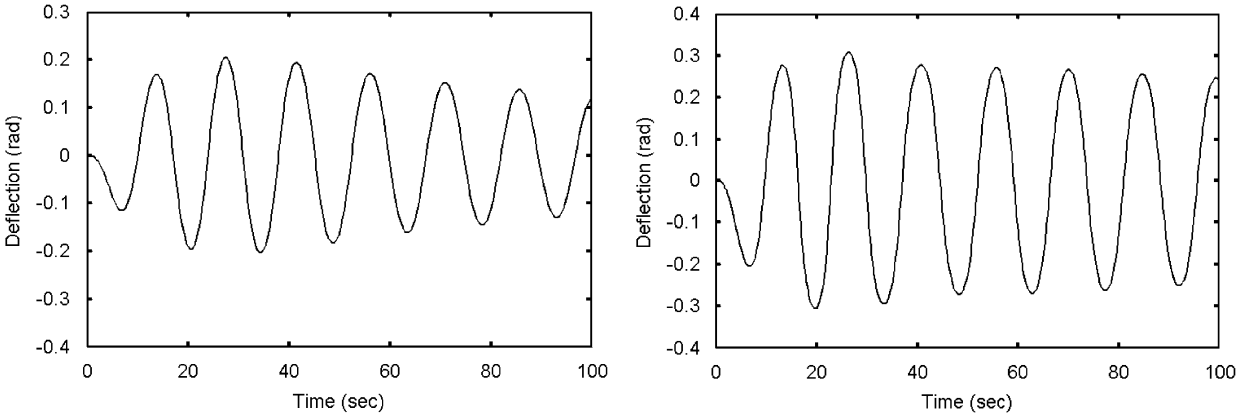

Fig. 8. Time response of the absorber with initial velocity 1.5×10^{-3} rad/s (left) and 3×10^{-3} rad/s (right).

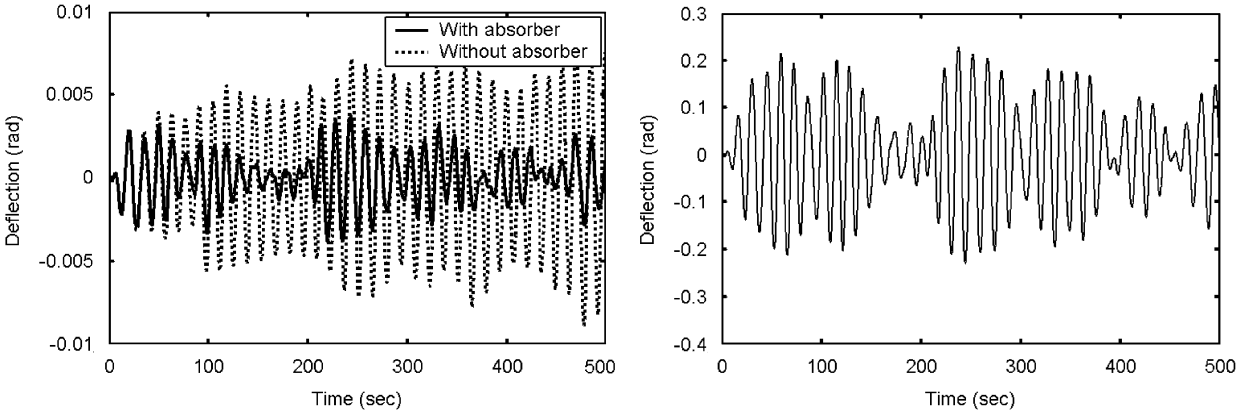

Fig. 9. Time response of the tower (left) and the absorber (right) in the case of random excitation.

beyond the scope of this study. Instead of this, the random white noise external moment is applied to the structures.

The response of the tower induced by wave load has been studied in Ref. [24], which shows that the maximum tower response is about 5×10^{-3} rad due to significant wave height of 15 m. Therefore, the white noise intensity is chosen to make the same scale of the tower response. Fig. 9 shows the time response of the tower's deflection and absorber's deflection induced by the random white noise external moment. The figure shows that the mass–spring inverted-pendulum-type DVA also has good effect in case of random excitation. DVA's deflection is still in safety region ($|\theta_d| < \pi/6 \approx 0.52$ rad).

7. Conclusion

The purpose of this paper is to study the vibration reduction for a stable inverted pendulum with passive mass–spring-pendulum-type DVA. Optimal parameters for DVA are chosen in order to maximize the damping properties of DVA–primary structure system. The result obtained shows the relationship between DVA's effectiveness and its location. There is a location of DVA, where the vibration of main structure has no excitation on DVA and DVA has no effect at all. In a numerical simulation of the inverted pendulum structure in the ocean, the idea of mass–spring inverted-pendulum-type DVA is proposed. The stability is analyzed by Lyapunov criterion in linear case and by cell-to-cell mapping method in general nonlinear case. It is obtained that the proposed type DVA has good effect in reducing free vibration and forced vibration due to white noise excitation. The influence of wave load, beam stiffness, damping at the pivot, added mass, mass of supported rod for inverted DVA and other effects may be subjects for further investigations. The problem will be more sophisticated for unstable inverted pendulum systems.

Acknowledgement

This work is completed partly with the financial support from the Vietnam National Council of Natural Science.

References

[1] J.P. Den Hartog, *Mechanical Vibration*, fourth ed., McGraw-Hill, New York, 1956, pp. 87–106.
[2] J.C. Snowdon, *Vibration and Shock in Damped Mechanical System*, Wiley, New York, 1968.
[3] R.G. Jacquot, D. Hoppe, Optimal random vibration absorbers, *Journal of Engineering Mechanics Division, American Society of Civil Engineers* 99 (1973) 612–616.
[4] B.G. Korenev, L.M. Reznikov, *Dynamic Vibration Absorbers: Theory and Technical Applications*, Wiley, New York, 1993.
[5] H. Matsuhisa, J.G. Park, Differential-pulley-type dynamic vibration absorber, *Proceedings of Asia-Pacific Vibration Conference*, 2001, pp. 451–455.
[6] X. Chen, A. Kareem, Efficacy of tuned mass dampers for bridge flutter control, *Journal of Structural Engineering, ASCE* 0733-9445 (2003) 1291–1300.
[7] H. Matsuhisa, R. Gu, Y. Wang, O. Nishihara, S. Sato, Vibration control of a ropeway carrier by passive dynamic vibration absorbers, *JSME International Journal (Series C)* 38 (4) (1995) 657–662.
[8] S.R. Bishop, D.J. Sudor, The 'not quite' inverted pendulum, *International Journal of Bifurcation Chaos* 19 (1) (1999) 273–285.
[9] H. Niemann, J.K. Poulsen, Analysis and design of controllers for a double inverted pendulum. *Proceedings of the American Control Conference,* Denver, CO, USA, 2003, pp. 2903–2808.
[10] H. Su, C.A. Woodham, On the uncontrollable damped triple inverted pendulum, *Journal of Computational and Applied Mathematics* 151 (2) (2003) 425–443.
[11] C. Anderson, Learning to control an inverted pendulum using neural network, *IEEE Control Systems Magazine* (1989) 31–36.
[12] V. Williams, K. Matsuoka, Learning to balance the inverted pendulum using neural networks, *Proceedings of the International Joint Conference on Neural Networks*, Singapore, 1993, pp. 214–219.
[13] A. Bradshaw, J. Shao, Swing-up control of inverted pendulum system, *Robotica* 14 (1996) 397–405.
[14] E. Koyanagi, S. Iida, K. Kimoto, S. Yuta, A wheeled inverse pendulum type self-contained mobile robot and its two-dimensional trajectory control, *Proceedings of ISMCR'92*, 1992, pp. 891–898.
[15] O. Matsumoto, S. Kajita, K. Tani, Attitude estimation of the wheeled inverted pendulum using adaptive observer, *Proceedings of 9th Academic Conference of the Robotics Society of Japan*, 1991, pp. 909–910 (in Japanese).

[16] Y. Yavin, C. Fragos, On a horizontal version of the inverted pendulum, *Computational Methods in Applied Mechanical Engineering* 121 (1997) 297–309.
[17] C.K. Chow, D.H. Jacobson, Studies of human locomotion via optimal programming, *Mathematical Bioscience* 10 (1971) 239–306.
[18] D. McRuer, Human dynamics in man–machine systems, *Automatica* 16 (1980) 237–253.
[19] B. Widrow, T. Viral, An adaptive (broom balancer) with visual inputs, *Proceedings of the IEEE International Conference on Neural Networks*, San Diego, II-641–II-647, CA, 1998.
[20] H. Hemami, F.C. Weimer, C.S. Robinson, C.W. Stockwell, V.S. Cvetkovic, Biped stability considerations with vestibular models, *IEEE Transactions on Automatic Control* 23 (1978) 1074–1079.
[21] D.T. Higdon, R.H. Cannon, On the control of unstable multiple-output mechanical systems, *ASME Publications* 63-WA-48 (1963) 1–12.
[22] W.-H. Wu, Equivalent fixed-base model for soil–structure interaction systems, *Soil Dynamics and Earthquake Engineering* 16 (1997) 323–336.
[23] P. Dong, H. Benaroya, T. Wei, Integrating experiments into an energy-based reduced-order model for vortex-induced-vibrations of a cylinder mounted as an inverted pendulum, *Journal of Sound and Vibration* 276 (2004) 45–63.
[24] P. Bar-Avi, H. Benaroya, Non-linear dynamics of an articulated tower submerged in the ocean, *Journal of Sound and Vibration* 190 (1996) 77–103.
[25] P. Bar-Avi, H. Benaroya, Stochastic response of a two DOF articulated tower, *International Journal of Non-Linear Mechanics* 32 (4) (1997) 639–655.
[26] S.K. Chakrabarti, D.C. Cotter, Motion analysis of articulated tower, *Journal of the Waterway, Port Coastal and Ocean Division, ASCE* 105 (1979) 281–292.
[27] O. Gottlieb, C.S. Yim, R.T. Hudspeth, Analysis of non-linear response of an articulated tower, *International Journal of Offshore and Polar Engineering* 2 (1992) 61–66.
[28] J.G. Park, H. Matsuhisa, Y. Honda, Vibration reduction of pendulum by dynamic vibration absorber with a differential pulley, *Transactions of the Japan Society of Mechanical Engineers* 67 (657) (2001) 1409–1415.
[29] C.S. Hsu, *Cell-to-Cell Mapping: A Method of Global Analysis for Nonlinear Systems*, Springer, New York, 1987.